9-2018

Measuring the practical particle-in-a-box: orthorhombic perovskite nanocrystals

Brandon Mitchell
West Chester University of Pennsylvania, bmitchell@wcupa.edu

Eric Herrmann
West Chester University of Pennsylvania

Junhao Lin
National Institute of Advanced Industrial Science and Technology, Japan

Leyre Gomez
University of Amsterdam

Chris de Weerd
University of Amsterdam

See next page for additional authors

Recommended Citation

Mitchell, B., Herrmann, E., Lin, J., Gomez, L., de Weerd, C., Fujiwara, Y., Suenaga, K., & Gregorkiewicz, T. (2018). Measuring the practical particle-in-a-box: orthorhombic perovskite nanocrystals. *European Journal of Physics, 39*(5), 1-12. http://dx.doi.org/10.1088/1361-6404/aac808

IOP Publishing European Journal of Physics
Eur. J. Phys. 39 (2018) 055501 (12pp) https://doi.org/10.1088/1361-6404/aac808

Measuring the practical particle-in-a-box: orthorhombic perovskite nanocrystals

Brandon Mitchell[1], Eric Herrmann[1], Junhao Lin[2], Leyre Gomez[3], Chris de Weerd[3], Yasufumi Fujiwara[4], Kazutomo Suenaga[2] and Tom Gregorkiewicz[3,4]

[1] Department of Physics, West Chester University, West Chester, PA 19383, United States of America
[2] National Institute of Advanced Industrial Science and Technology (AIST), AIST Central 5, Tsukuba 305-8565, Japan
[3] Institute of Physics, University of Amsterdam, Science Park 904, 1098 XH Amsterdam, The Netherlands
[4] Division of Materials and Manufacturing Science, Graduate School of Engineering, Osaka University, 2-1 Yamadaoka, Suita, Osaka 565-0871, Japan

E-mail: bmitchell@wcupa.edu

Received 3 February 2018, revised 18 May 2018
Accepted for publication 25 May 2018
Published 27 June 2018

Abstract

A connection between condensed matter physics and basic quantum mechanics is demonstrated as we use the fundamental 3D particle-in-a-box model to explain the optical properties of semiconductor nanocrystals, which are substantially modified due to quantum confinement. We also discuss recent advances in the imaging and measurement capabilities of transmission electron microscopy, which have made it possible to directly image single nanocrystals while simultaneously measuring their characteristic absorption energies. We introduce the basic theory of nanocrystals and derive a simplified expression to approximate the optical bandgap energy of an orthorhombic nanocrystal. $CsPbBr_3$ perovskite nanocrystals are used to demonstrate this model due to their cubic crystal structure, large absorption cross-section, and favourable dielectric properties, which make them ideal for exploring the applications of this simple classroom problem. Various orthorhombic shapes are explored, and the predicted values of the optical bandgap energies using the proposed model are shown to be in good agreement with the experimentally determined values.

Supplementary material for this article is available online

Keywords: particle-in-a-box, nanocrystals, transmission electron microscopy

(Some figures may appear in colour only in the online journal)

1. Quantum confinement and nanocrystals

The properties of bound state quantum systems are among the most fundamental aspects of nature introduced to students in their study of quantum mechanics. When particles are confined to distances comparable to their De Broglie wavelengths, quantum behaviours begin to manifest. This has interesting consequences such as particles only being able to exist with discrete energies, where their ground state energy is non-zero and increases as the confinement of the particle becomes more severe. If the particle is confined in all three dimensions (the so-called 'particle-in-a-box'), each confinement direction influences the values of the energy levels. Despite being an idealised system, the particle-in-a-box model has been very successful to estimate the behaviours of more complex quantum systems. For example, the basic optical properties of semiconductor quantum dots and nanocrystals (NCs) can be explained quite accurately by primarily considering the effects of quantum confinement induced by an infinite potential [1–4], which makes the particle-in-a-box the ideal system for demonstrating the utility of these fundamental models [1, 5–8][5].

Nanocrystals have been studied for several decades due to their unique properties, and they are emerging in medical and renewable energy applications as well as high-energy detection and high-resolution displays such as quantum-dot-LED (Q-LED) TVs [9–14]. For medical purposes, NCs are being explored as a means to release drugs under tissue and as markers for imaging. In renewable energy applications, NCs have the potential to modify the solar spectrum and make use of previously wasted wavelengths of light emitted by the Sun. These applications are possible because the wavelength of light that can be absorbed and emitted from NCs depends primarily on the size of the nanocrystal for most materials. The entire visible spectrum can be emitted from an ensemble of NCs made of a single material simply by changing the size of the nanocrystals [3, 13]. Utilising the high spatial and energy resolution of scanning transmission electron microscopy (STEM) techniques, it is possible to simultaneously measure the dimensions and optical properties of a nanocrystal [4, 15, 16]. We will discuss the fundamentals of these measurement techniques and show that they can be used to provide valuable insights on the relationship between the size of NCs and their optical properties, in a transparent and pedagogically useful manner that provides a valuable connection between condensed matter physics and quantum mechanics.

2. Carrier confinement in nanocrystals: theoretical background

There are two ways to model a semiconductor NC [6]: one is to think of a NC as a large cluster, where atoms are added until a certain sized cluster is achieved. The second is to think of the NC as a bulk semiconductor that has been reduced in size, such that mobile electrons in the semiconductor are strongly confined by the edges. The latter approach will be used in this manuscript. Therefore, we will first review some of the basic principles of bulk semiconductor materials and then extend our discussion to nanocrystals. A single atom is characterised by its unique set of discrete energy levels, but when two atoms are placed close together, the interaction between the electrons and nuclei of the atoms causes the allowed energy levels to split. As the number of interacting atoms increases, so does the splitting of the allowed energy

[5] The validity of using ideal quantum systems to explain real-world phenomena, as well as its pedagogical importance have been investigated and discussed by other authors [7, 8].

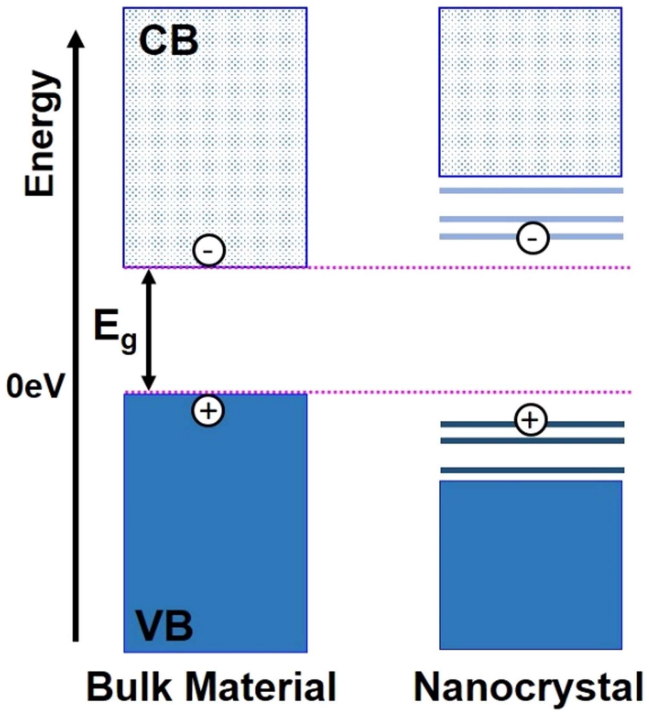

Figure 1. Comparison of the bandgap energy E_g for a bulk semiconductor versus a NC made from that material. The confinement of the electrons and holes in the NC widens the bandgap and introduces an atomic energy level structure.

levels. In a solid crystal material, the atoms are arranged in a periodic array known as the crystal lattice. When millions of atoms come together to form a crystal, the large number of interactions between the electrons and nuclei lead to a near continuum of allowable energy levels, called energy bands. Similar to the single atom case, there are both allowed and forbidden energy bands in a solid, where the range of forbidden energy states situated between allowed energy bands are known as bandgaps.

The allowed energy bands are filled by electrons that originate from each atom in the solid, and the highest energy band that is completely filled at absolute zero (0 K) is called the valence band (VB). The lowest energy band that is not fully (metals) or completely (insulators) unoccupied is called the conduction band (CB). The energy difference between the VB and CB is called the *fundamental* bandgap of the material. For metals, the CB is partially filled even at 0 K, which is why electrons are able to 'move freely' in a metal. In a semiconductor, the CB is empty at 0 K, but the bandgap is small enough that the thermal energy available at room temperature can be sufficient for an electron to reach it.

Another way to move an electron from the VB to the CB is to excite the semiconductor with a photon that has energy greater than the bandgap, which can then transfer its energy to the electron (figure 1). The VB can then be thought of as a filled band, but with a positively charged 'hole' left behind. If the excitation provides more energy than the bandgap, the electron and hole can move inside of the material. Near the bottom of the conduction band for electrons and the top of the valence band for holes, these particles are described as '(nearly) free particles' with effective masses (m_e^* and m_h^*), which account for their interactions with

the crystal lattice [5, 6, 17, 18]. For example, if it is more difficult for an electron in a material to be accelerated than a free electron, then the effective mass of the electron in the material will be greater than the electron mass in vacuum.

The electron will eventually return to the valence band, taking the place of a hole and emitting a photon with an energy equal to the bandgap energy. When a NC is excited, an electron will also be promoted into the conduction band and will leave behind a hole, except that the electron and hole will then be spatially confined by the dimensions of the NC and, if the dimensions are small enough, quantum confinement effects will become significant. Thus, the electron and hole are 'particles in a box', but also interact with the crystal lattice, which both contribute to their allowed energy values. Typically, NCs are assumed to be spherical and therefore the confinement is estimated as an infinite spherical potential. The calculation for the energy eigenvalues of a particle confined to an infinite spherical well of radius (r) is a standard textbook problem, which yields the expression

$$E^{nl}_{\text{sphere}}(r) = \frac{\hbar^2 \chi^2_{nl}}{2mr^2}, \tag{1}$$

where χ_{nl} are the zeros of the Bessel function. This confinement energy is negative for holes and positive for electrons. Since the electron and the hole occupy the CB and VB, respectively, the CB will be shifted up in energy, while the VB will be shifted down in energy. This will widen the bandgap of the material by the combined confinement energy of the electron and the hole:

$$E^{nl}_{\text{conf, sphere}}(r) = \frac{\hbar^2 \chi^2_{nl}}{2m_e^* r^2} + \frac{\hbar^2 \chi^2_{nl}}{2m_h^* r^2}. \tag{2}$$

The widening of the bandgap occurs in discrete increments for different values of n and l, which is illustrated in figure 1. Taking the electron and hole to be in the ground state of the spherical well potential ($n = 1$ and $l = 0$) for both the electron and the hole and adding it to the bulk crystal bandgap energy, one can estimate the *fundamental* optical bandgap of the NC as

$$E_{OG}(r) = E_{G,\text{bulk}} + E_{\text{conf,sphere}}(r) = E_{G,\text{bulk}} + \frac{\hbar^2 \pi^2}{2r^2} \cdot \left[\frac{1}{m_e^*} + \frac{1}{m_h^*}\right]. \tag{3}$$

While equation (3) describes the fundamental bandgap, it is clear in figure 1 that there are other atomic-like levels where the electron and hole are not in their ground states. Inter-band transitions between these levels can also occur in nanocrystals, leading to emission lines with *higher* energies than the bandgap, which is not typically observed in bulk semiconductors.

2.1. The cubic nature of $CsPbBr_3$ perovskite NCs

Halide perovskite NCs currently receive considerable attention as new materials for solar energy conversion, high-energy detection and display purposes [4, 10–12]. Unlike many NCs that form spherical nanoclusters, perovskites such as $CsPbBr_3$ have a cubic crystal structure and form NCs with a cubic geometry, which is illustrated in figure 2(a). This cubic structure can clearly be seen in figure 2(b), which shows STEM images of ensembles of $CsPbBr_3$ NCs, as well as isolated NCs. Due to their cubic geometry, the spherical potential that is normally assumed to describe quantum confinement is less appropriate when modelling $CsPbBr_3$ or other cubic perovskite NCs. When an electron is promoted into the conduction band in a cubic NC, the electron and the hole will be spatially confined to an orthorhombic potential.

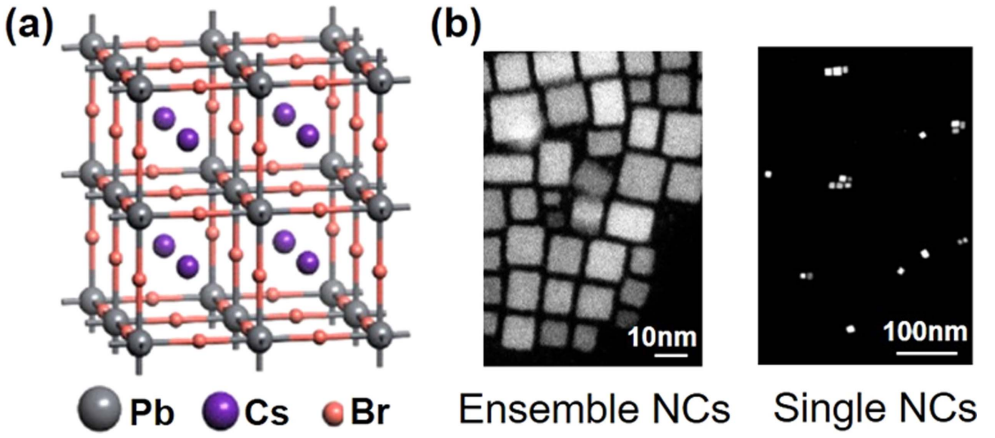

Figure 2. (a) The atomic structure of bulk $CsPbBr_3$. (b) STEM images of $CsPbBr_3$ NCs both in ensembles and isolated.

To account for the cubic geometry, we must consider a particle-in-rectangular potential with unequal side lengths. The 3D infinite rectangular potential is well-studied in introductory quantum mechanics, and detailed solutions for the energy eigenvalues are given in several textbooks [5, 19–22]. Following the same procedure used for the spherical potential mentioned above, the orthorhombic confinement energy term, including the contribution from the electron and the hole, becomes

$$E_{\text{Orthom}}^{\text{conf}} = \frac{\hbar^2\pi^2}{2m_e^*}\cdot\left[\frac{n_x^2}{a^2}+\frac{n_y^2}{b^2}+\frac{n_z^2}{c^2}\right]+\frac{\hbar^2\pi^2}{2m_h^*}\cdot\left[\frac{n_x^2}{a^2}+\frac{n_y^2}{b^2}+\frac{n_z^2}{c^2}\right], \tag{4}$$

where a, b and c are the lengths of the sides of the rectangular potential. The *fundamental* optical bandgap for an orthorhombic NC then takes the form

$$E_{OG}(a,\,b,\,c) = E_{G,\text{bulk}} + \frac{\hbar^2\pi^2}{2\mu^*}\cdot\left[\frac{1}{a^2}+\frac{1}{b^2}+\frac{1}{c^2}\right], \tag{5}$$

where μ^* is the average effective mass of the electron and hole, given as

$$\mu^* = \left[\frac{1}{m_e^*}+\frac{1}{m_h^*}\right]. \tag{6}$$

Equation (5) will be used to estimate the optical bandgap of orthorhombic $CsPbBr_3$ NCs. Also, the NCs discussed in this work have ligand-terminated surfaces such that the effect of surface defects on the energy structure is minimised. These NCs were fabricated using the same procedure that is described in detail in other reports [4, 11]. In the next section, we will introduce the fundamentals of STEM and electron energy loss spectroscopy. These techniques will be used to measure the physical dimensions and optical bandgaps of various NCs, which will then be compared with values predicted by equation (5).

3. Measuring the bandgap of a single cubic NC using electron energy loss spectroscopy

Photoluminescence is commonly used to measure the optical bandgap of bulk semiconductors, where a light source is used to excite electrons from the VB into the CB. The light that is subsequently emitted from the material is then collected using a detector. However, the size of most NCs prohibits optical techniques since the wavelength of light is nearly two orders of magnitude larger than the size of the NCs, and thus it is impossible to resolve a NC spatially with any reasonable certainty. In a similar way, it would not be possible to use optical excitation to excite a single NC and measure only its absorption properties. It is possible to use optical excitation sources to probe large ensembles of NCs [11]; however, the bandgap energy of a single NC in an ensemble was found to be influenced by the surrounding NCs [4], and thus only an average optical bandgap can be determined using this technique.

In order to image a single NC, a STEM can be used, where a focused beam of high-energy electrons ($\sim$100 KeV) is scanned across the sample. The De Broglie wavelength of a high-energy electron is very small ($\sim$0.004 nm) and can therefore be used to resolve nanoscale objects such as NCs. As electrons move through the sample, they can scatter with the atoms in the material either elastically or inelastically and are collected by a detector on the other side. There are two primary detection geometries used in STEM, annular dark field (ADF) detection and bright-field detection; however, we will only focus on ADF detection in this work. For ADF detection, a ring-shaped detector with a hole in the middle is used. Electrons that pass through the sample without significant deflection will not be collected (no signal), while electrons that are scattered from atoms within the material will be collected by the ring-shaped detector (signal). As the number of scattered electrons increases, so does the intensity of the signal. Heavier atoms will deflect more electrons than light atoms; therefore, the heavier atoms will appear brighter in the image. The resulting contrast between heavy and light atoms is referred to as *Z*-contrast and can be used to identify atoms within the lattice. The thickness of a sample can also be estimated using *Z*-contrast ADF images, since the image intensity is related to sample thickness. This is because electrons are more likely to be scattered if they pass through thicker samples of the same material; thus thicker samples will appear brighter than thinner samples in the *Z*-contrast ADF images. Using the relative image intensity between samples, the thickness of each sample can be estimated [4].

In addition to detecting electrons for imaging purposes, the energy of electrons that are scattered can be measured by using an electron spectrometer. In an electron spectrometer, a magnetic field is present and electrons are deflected via the Lorenz force. From these deflections, the energy of an electron that entered the spectrometer can be determined. If the electron scatters inelastically from the material, some of the electron's energy will be lost. Certain energy losses can be correlated with different 'events' that occur within the material. By measuring the intensity of electrons over a range of energy loss values, structural, optical and chemical information can be obtained such as lattice vibrational modes, intra- and inter-band transition energies, plasmon resonances and inner shell ionisation energies. This type of measurement is called electron energy loss spectroscopy, or EELS. Recent advances in STEM now allow EELS to be performed with an ultra-high-energy resolution on the order of 10 meV, while simultaneously imaging a single NC with sub-nanometer spatial resolution [4, 15, 16].

Next, we will explain the basic features of EEL spectra. In a thin sample, most of the electrons either do not scatter from the material or do so elastically, and therefore there is no energy loss. These electrons give rise to the zero loss peak, which is set to 0 eV on the *x*-axis of an EEL spectra. The zero loss peak of a $CsPbBr_3$ nanocrystal is shown in figure 3(a). The

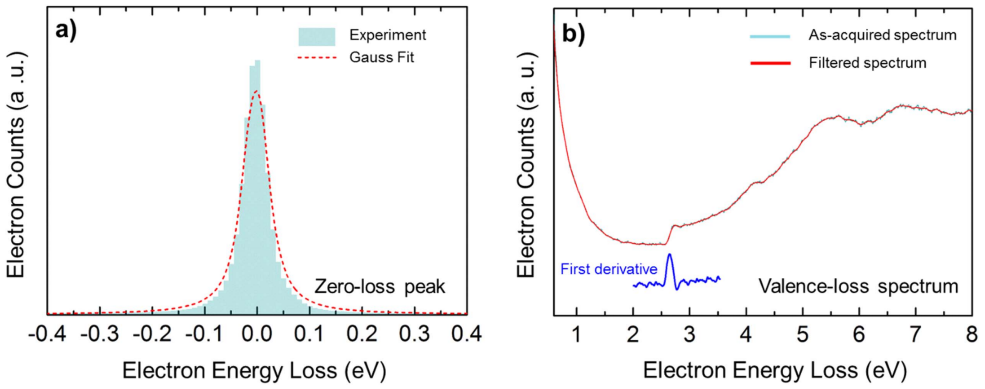

Figure 3. (a) Zero loss EEL spectra of a $CsPbBr_3$ nanocrystal, which corresponds to electrons that did not scatter from the nanocrystals, or did so elastically, along with a Gaussian fit of the data. (b) The low-loss or valence-loss spectra of the same nanocrystal. The data was smoothed out using a Savitzky–Golay filter, and the first derivative of the smoothed line was taken. The optical bandgap of the nanocrystal can be estimated from the energy loss value where the electron counts first begin to increase, which is indicated by the peak of the first derivative and has a value of ∼2.60 eV for this NC.

width of the zero loss peak gives information on the distribution of energies of the electrons in the beam, which usually exhibits a Gaussian behaviour [23]. By fitting the zero loss peak and evaluating the full width at half maximum (FWHM), the energy resolution of the measurement can be estimated. In the valence-loss spectrum (figure 3(b)), the tail of the zero loss peak can be observed on the left. For this NC, an abrupt increase in the electron count is observed at an energy loss of ∼2.60 eV, which is due to an interaction that causes an electron to be excited across the optical bandgap of the NC. Thus, this energy loss value can be used to determine the optical bandgap of the material, which is in principle analogous to how bandgap energies are determined in optical absorption spectroscopy [24, 25]. To more accurately determine this energy loss value, the as-acquired data can be digitally smoothed using a Savitzky–Golay filter [26]. The first derivative (the slope of the curve) of the smoothed function can then be taken. The step-like increase appears as a peak in the first derivative, which can be fit with a Gaussian curve. The bandgap energy of the NC can then be estimated from the apex of the fit peak, and the FWHM of the peak can be used to estimate the experimental error. Thus, based on this EEL spectrum, the optical bandgap of this NC would be reported as 2.60 ± 0.03 eV. It should be noted that there are several wavy features for electron loss energies greater than 3.5 eV in figure 3(b). These correspond to electron/hole excitation higher into the bands, and are also observed in optical absorption measurements performed on nanocrystals [11]. Information on the equipment and settings used in these experiments, as well as the synthesis of the nanocrystals, can be found in the supporting information document is available online at stacks.iop.org/EJP/39/055501/mmedia.

Figure 4(a) shows the valence-loss or low-loss EEL spectra for three nearly cubic NCs of various sizes with the corresponding ADF *Z*-contrast STEM images. The exponential decay observed for energies lower than 2.3 eV in the EEL spectra is the tail from the zero loss peak signal, which was not included as it is much stronger than the signal from the absorption edge. The bandgap energy is identified as the energy when the decay of the zero loss signal ceases and an abrupt increase in the EELS signal is observed. Due to the size of the nanocrystals,

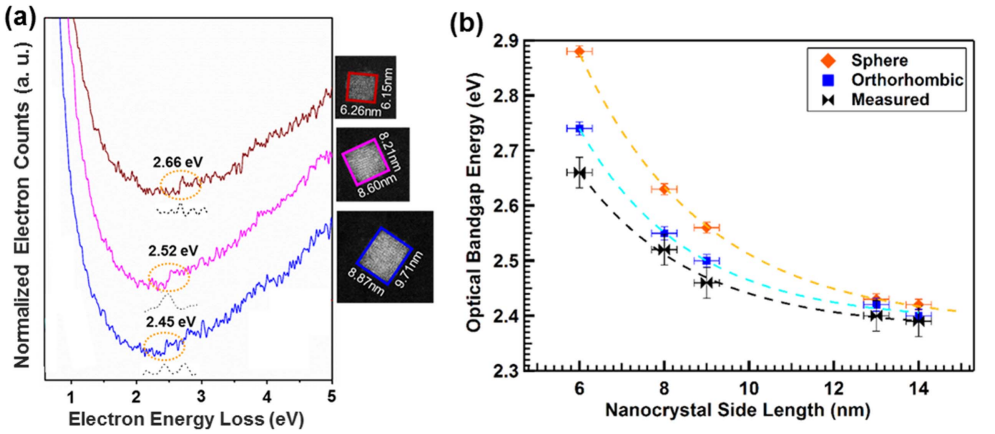

Figure 4. (a) Valence-loss EEL spectra for cubic NCs with different side lengths. The bandgap energy is easier to identify by using the first derivative of the EEL spectral curves, which is given by the dotted black curves below each spectra. Peaks in the first derivative near the onset on the absorption indicate the bandgap energy of the NC. (b) Optical bandgap energy plotted against the side length of cubic NCs. The measured values are plotted as well as those calculated by assuming a spherical shape (equation (3)) and an orthorhombic shape (equation (5)).

very few electrons will interact with the NC, and the signal does not increase significantly, which can make it difficult to identify the energy where the onset of the bandgap absorption occurs. To make this more evident, the first derivative of the smoothed EELS signal is used. The first derivative curve is plotted in dotted black lines below the EEL spectra in figure 4(a). Since the first derivative is sensitive to changes in the slope of the EEL spectral curve, several bumps may be present in the first derivative curve. Therefore, one must identify where the decay from the zero loss peak stops, and look for a peak in the first derivative at that point, which is typically larger than the other peaks that are due to random fluctuations in the signal.

As expected from equation (5), the EELS absorption edge appears at lower energies for larger NCs. The measured optical bandgaps for several nearly cubic NCs are plotted versus side length in figure 4(b). The bandgaps estimated using equation (3) (spherical potential) and equation (5) (cubic potential) are also plotted. In these calculations, the value of the bulk $CsPbBr_3$ bandgap energy was taken as the average of values reported by various groups [4, 10–12, 27]. The effective masses of the electron and the hole were taken to be 0.15 m_e and 0.14 m_e, respectively, where m_e is the mass of a free electron [11, 27]. While the notion of an effective mass can only be properly defined in an infinite system, these values are commonly used as approximations when estimating their confinement energy. The error bars for the measured bandgap values are estimated from the FWHM of the zero loss peak in the EEL spectra, while the errors in the calculated values are estimated from the standard deviation in the values of the reported bandgap energies and effective masses [4, 10–12, 27].

Theoretically, the confinement energy for a spherical potential is ∼30% higher than a cubic potential of the same length scale and with all other parameters kept the same. Experimentally, it is evident that the spherical potential significantly overestimates the confinement effect, especially for small NCs, while the cubic potential estimates the measured optical bandgap reasonably well within uncertainty. In the next section it will be shown that an orthorhombic potential will prove essential for explaining the behaviour of non-cubic NCs.

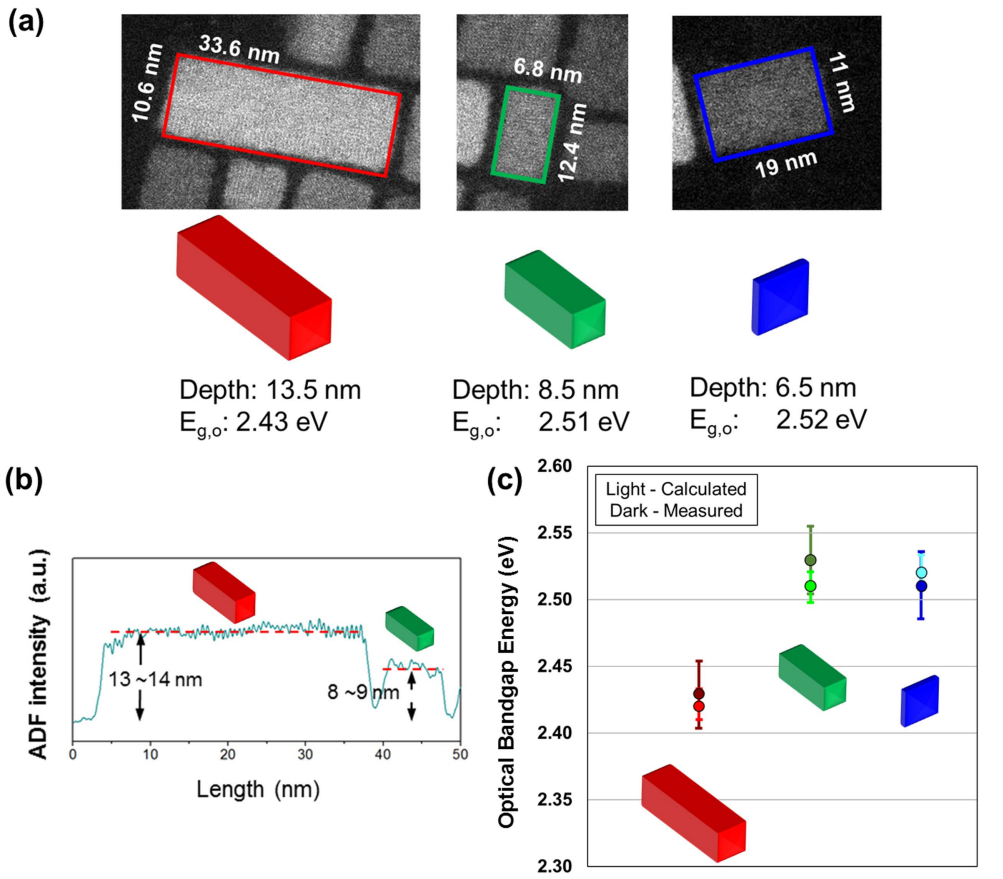

Figure 5. (a) STEM images of NCs with three different shapes: (1) long rod, (2) short rod, and (3) platelet. The depths are included for each shape as determined using *Z*-contrast ADF imaging, as well as their corresponding measured energy bandgaps. (b) ADF intensity across the long rod and the short rod. The thicknesses of the NCs are estimated based upon the relative intensities compared to a reference sample [4]. (c) Plot of the measured energy bandgaps (dark colours) and the bandgaps calculated using equation (5) (light colours).

4. Bandgap evaluation for non-cubic NCs

Several NCs were found that did not have a near cubic structure, such as the three NCs shown in figure 5(a), which have a rod-like or platelet geometry. Figure 5(b) shows the ADF intensity across a long and a short rod. The thicknesses of these NCs are then estimated based from statistics and upon their relative intensities, as compared to a reference sample [4]. Although the platelet has a rather large area in the *x*–*y* plane, its depth was estimated to be only ∼6.5 nm. The short rod was found to have an *x*–*y* dimension of 6.8 × 12.4 nm, with a depth of ∼8.5 nm, and the longer rod had an *x*–*y* dimension of 33.6 × 10.6 nm, with a depth of ∼13.5 nm. The optical bandgap measured for the platelet and the short rod are quite similar despite the differences in their respective dimensions. The measured optical bandgaps of the NCs are plotted with the values obtained from equation (5) in figure 5(c), which are in good agreement.

It is clear that using a simple spherical potential to account for the confinement effects in NC with non-cubic geometries would be a challenge. What would one choose for the radius of the NC? From figure 3(b), it can be seen that if the radius were set as the largest dimension, the confinement would be underestimated. On the other hand, if the radius was chosen to be the smallest dimension, the confinement would be overestimated. In addition, the larger dimensions are small enough that they still provide a significant degree of confinement. Thus, the platelet and rod could not be treated as systems with a lower dimension of confinement. For example, if the platelet were treated as a quantum well with confinement only in one dimension, the optical bandgap would be underestimated. Thus, the orthorhombic potential is necessary for estimating the optical bandgap of orthorhombic NCs to a reasonable degree.

Of course, the formulation used in this article is a simplification of the situation. In the derivation of equations (3) and (5), the electron and hole were assumed to be non-interacting particles. To account for the interaction between them in a semiconductor, a full two particle Hamiltonian would have to be solved. Several authors have performed this calculation for a spherical geometry, and have shown that two correction terms are introduced, which take into account the Coulomb interaction between the electron and the hole, and the energy arising from the spatial correlation between the electron and hole [5, 6, 28, 29][6]. The magnitude of these two correction terms is dependent on the dielectric constant of the semiconductor, and can be ignored when the dielectric constant is large. One of the additional benefits of $CsPbBr_3$ NCs is that they have a relatively high dielectric constant and therefore these correction terms are negligible in this system [11]. It should also be noted that spatial confinement is not the only method used to modify the optical bandgap of halide perovskites, which have the form $CsPb(X)_3$. The bandgap of these materials is also very sensitive to elemental substitutions. For example, if Br is replaced with other elements such as Cl or I, the bandgap of the bulk material changes from $\sim$2.34 eV ($CsPbBr_3$) to $\sim$3.1 eV ($CsPbCl_3$) and $\sim$1.8 eV ($CsPbI_3$) [12]. The optical bandgap of these perovskites can then be fine-tuned using spatial confinement.

5. Conclusions

Quantum dots and nanocrystals are useful systems for providing a clear illustration of the quantum confinement effects in practice. The ability to simultaneously measure the physical dimensions and the bandgap energy of NCs enabled by the recent advances of STEM and EELS provides a unique means to explore the influence of quantum confinement on the optical properties of semiconductors. $CsPbBr_3$ perovskite NCs serve an ideal system to probe these effects due to their strong absorption (direct bandgap structure), cubic geometry and high dielectric constant, which reduces the influence of Columbic and polarisation effects between the electrons and holes. As a result, the confinement effect can be estimated by using a simple particle-in-a-box model and can explain the correlation between the size and shape of the NCs and their optical bandgaps in a transparent way.

[6] Equation (3) was not derived for embedded quantum dots or self-assembled quantum dots with a paraboloid shape. For information on these systems, see [1].

Acknowledgments

JL and KS thank the financial support from the Japan Science and Technology Agency (JST)-ACCEL and the Japan Society for the Promotion of Science (JSPS) KAKENHI (Grants No. JP16H06333 and No. P16823).

ORCID iDs

Brandon Mitchell https://orcid.org/0000-0003-1774-5693

References

[1] Riel B J 2008 An introduction to self-assembled quantum dots *Am. J. Phys.* **76** 750–7
[2] Chukwuocha E O, Onyeaju M C and Harry T S T 2012 Theoretical studies on the effect of confinement on quantum dots using the Brus equation *World J. Condens. Matter Phys.* **2** 96–100
[3] Amiri G R, Fatahian S and Mahmoudi S 2013 Preparation and optical properties assessment of CdSe quantum dots *Mater. Sci. Appl.* **4** 134–7
[4] Lin J, Gomez L, de Weerd C, Fujiwara Y, Gregorkiewicz T and Suenaga K 2016 Direct observation of band structure modifications in nanocrystals of $CsPbBr_3$ perovskite *Nano Lett.* **16** 7198–202
[5] Gaponenko S V 2010 *Introduction to Nanophotonics* (Cambridge: Cambridge University Press)
[6] Koole R, Groeneveld E, Vanmaekelbergh D, Meijerink A and de Mello Donegá C 2014 Size effects on semiconductor nanoparticles *Nanoparticles* ed C de Mello Donegá (Berlin: Springer)
[7] Burt M G 1994 On the validity and range of applicability of the particle in a box model *Appl. Phys. Lett.* **65** 717–9
[8] Belloni M and Robinett R W 2014 The infinite well and Dirac delta function potentials as pedagogical, mathematical and physical models in quantum mechanics *Phys. Rep.* **540** 25–122
[9] Timmerman D, Izeddin I, Stallinga P, Yassievich I N and Gregorkiewicz T 2008 Space-separated quantum cutting with silicon nanocrystals for photovoltaic applications *Nat. Photon.* **2** 105–9
[10] Stoumpos C C *et al* 2013 Crystal growth of the perovskite semiconductor $CsPbBr_3$: a new material for high-energy radiation detection *Cryst. Growth Des.* **13** 2722–7
[11] Protesescu L, Yakunin S, Bodnarchuk M I, Krieg F, Caputo R, Hendon C H, Yang R X, Walsh A and Kovalenko M V 2015 Nanocrystals of cesium lead halide perovskites (CsPbX3, X = Cl, Br, and I): novel optoelectronic materials showing bright emission with wide color gamut *Nano Lett.* **15** 3692–6
[12] Beal R E, Slotcavage D J, Leijtens T, Bowring A R, Belisle R A, Nguyen W H, Burkhard G F, Hoke E T and McGehee M D 2016 Cesium lead halide perovskites with improved stability for tandem solar cells *J. Phys. Chem. Lett.* **7** 746–51
[13] Lim X 2016 The nanoscale rainbow *Nature* **531** 26–8
[14] Yang Z *et al* 2017 Impact of the halide cage on the electronic properties of fully inorganic cesium lead halide perovskites *ACS Energy Lett.* **2** 1621–7
[15] Tizei L H G, Lin Y, Mukai M, Sawada H, Lu A, Li L, Kimoto K and Suenaga K 2015 Exciton mapping at subwavelength scales in two-dimensional materials *Phys. Rev. Lett.* **114** 107601
[16] Sasaki T, Sawada H, Hosokawa F, Sato Y and Suenaga K 2014 Aberration-corrected STEM/TEM imaging at 15 kV *Ultramicroscopy* **145** 50–5
[17] Kittel C 2004 *Introduction to Solid State Physics* 8th edn (New York: Wiley)
[18] Simon S H 2013 *The Oxford Solid State Basics* (Oxford: Oxford University Press)
[19] Eisenburg R and Resnick R 1985 *Quantum Physics of Atoms, Molecules, Solids, Nuclei, and Particles* 2nd edn (New York: Wiley)
[20] Griffiths D 2005 *Introduction to Quantum Mechanics* 2nd edn (Upper Saddle River, NJ: Pearson Education)
[21] Scherrer R 2006 *Quantum Mechanics: An Accessible Introduction* 1st edn (Reading, MA: Addison-Wesley)
[22] McIntyre D 2012 *Quantum Mechanics* 1st edn (San Francisco, CA: Pearson Education)

[23] Hofer F, Schmidt F P, Grogger W and Kothleitner G 2016 Fundamentals of electron energy-loss spectroscopy *IOP Conf. Ser.: Mater. Sci. Eng.* **109** 012007
[24] Erni R and Browning N D 2007 Quantification of the size-dependent energy gap of individual CdSe quantum dots by valence electron energy-loss spectroscopy *Ultramicroscopy* **107** 267–73
[25] Kapetanakis M D, Zhou W, Oxley M P, Lee J, Prange M P, Pennycook S J, Idrobo J C and Pantelides S T 2015 Low-loss electron energy loss spectroscopy: an atomic-resolution complement to optical spectroscopies and application to graphene *Phys. Rev.* B **92** 125147
[26] Savitzky A and Golay M J E 1964 Smoothing and differentiation of data by simplified least squares procedures *Anal. Chem.* **36** 1627–39
[27] Wu K, Liang G, Shang Q, Ren Y, Kong D and Lian T 2015 Ultrafast interfacial electron and hole transfer from $CsPbBr_3$ perovskite quantum dots *J. Am. Chem. Soc.* **137** 12792–5
[28] Brus L 1986 Electronic wave functions in semiconductor clusters: experiment and theory *J. Phys. Chem.* **90** 2555–60
[29] Kayanuma Y 1988 Quantum-size effects of interacting electrons and holes in semiconductor microcrystals with spherical shape *Phys. Rev.* B **38** 9797–805